13B.1 The effects of temperature on $\mathbf{Z_{dr}}$ calibration

J.C. Hubbert*, M. Dixon, G. Meymaris, and S. M. Ellis

National Center for Atmospheric Research, Boulder, CO

1. Introduction

The calibration of Z_{dr} typically consists of two parts: 1) calibration "snapshot" measurements, ideally accomplished over a very short time span and, 2) calibration maintenance measurements that track any drift in the snapshot calibration measurement over extended time intervals. The causes and the nature of the drift in the Z_{dr} snapshot calibration over time is not well understood and there are very few long term experimental measurements in the literature. Here the Z_{dr} variance for S-Pol over long time periods (multiple days) is investigated.

Recent Z_{dr} calibration efforts for S-Pol (and NEXRAD) have revealed a significant uncertainty or variability in the Z_{dr} calibration offset number (snapshot calibration number). In the past S-Pol Z_{dr} has been calibrated via vertical pointing (VP) data in light rain. As this implies, the VP technique is most tested for warm season precipitation. As an example of calibration for S-Pol, the Fig. 1 shows Z_{dr} bias estimated from VP measurements over about 3.5 months during the field campaign DYNAMO, 2011, in the Maldives. The measurements are very stable especially between the two dotted lines where the polarization switch was unchanged. The temperature at the S-Pol site ranged from 24.5° to 29.6° during these 23 measurements.

With the advent of FRONT (Front Range Observational Network Testbed), S-Pol was operated for 2014 - 2015 winter storms where light rain over the radar is indeed rare. The VP technique can be executed but there are several caveats: 1) winter storms are typically not very deep vertically and valid VP data are usually considered to begin at 2.5 km or more in range (i.e., height above the radar) due to near field effects and TR-tube[1] recovery, 2) the reflectivities of winter precipitation are typically fairly low, and 3) if the precipitation (snow flakes) has a small vertical velocity, then the clutter filter may affect the calculated Z_{dr} calibration number. Here we use the crosspolar power technique to calibrate Z_{dr} (Hubbert et al. 2003), which makes use of the principle of radar reciprocity. The principle of radar reciprocity states that the two crosspolar members of the radar scattering matrix are equal, i.e, $S_{hv} = S_{vh}$ (Saxon, D.S. 1955). In short this means that the two measured crosspolar powers should be equal. Using the crosspolar power technique (CP), we investigate the long term variance of Z_{dr} calibration.

Executing the CP requires solar power ratio measurements and crosspolar power ratio measurements either from clutter or precipitation targets. Historically these data were collected from two different scanning strategies. We have developed a measurement technique where both numbers can be gathered from just a single solar box scan. Since the transmitter is left on during solar scans, the crosspolar power ratio can be calculated from data from shorter ranges, where sidelobe ground clutter echo is present, and the solar power ratio can be calculated from longer ranges (i.e., > 100 km) where ground clutter and precipitation echoes are not present. Using CP, the Z_{dr} bias is estimated on several days over an extended period of time. Since the CP can be executed almost anytime during the daylight hours, CP can be executed repeatedly throughout the day (approximately 7 minute intervals). During the measurement periods, the temperature at S-Pol ranged from -20° C to 20° C and the Z_{dr} bias offset varied nearly 0.4 dB, which on average is 0.01 dB/(deg. C). Clearly such variations in the Z_{dr} calibration number need to be accounted for. Here we identify the radar components that are responsible for the observed variations in Z_{dr} calibration.

2. The Crosspolar Power Technique for $\mathbf{Z_{dr}}$ Calibration

S-Pol uses a single transmitter and a mechanical polarization switch to transmit alternate pulses of H (horizontal) and V (vertical) polarized waves. Two receivers are used to measure the copolar and crosspolar return signals (in contrast to H and V receivers), which is accomplished with an IF (intermediate frequency) switch. Because of the IF trans-

*NCAR/EOL, Boulder, Colorado 80307, email: hubbert@ucar.edu

[1] an electronic component that protects the receiver circuitry from the high power transmit pulse

fer switch, there are four possible paths through the receiver chain and thus four possible sun calibration numbers. Shown in Fig. 2 is a simplified block diagram of S-Pol where $P_{H,V}$ are the input transmitter powers, $C^T_{H,V}$ are the losses associated with the circulators on transmission, $C^R_{H,V}$ are the losses associated with the circulators on reception, $\mathrm{LNA}_{H,V}$ are the gains of the low noise amplifiers, $W_{H,V}$ are waveguide losses, $G^A_{H,V}$ are the antenna gains, $G^R_{H,V}$ are the receiver gains and $R_{co,x}$ are the received powers. The dotted line represents the measurement test plane where both the transmit (receive) power is monitored and test signals can be injected. From Fig. 2 it follows that,

$$Z^m_{dr} = \frac{P_H C^T_H W^2_H (G^A_H)^2 LNA_H\, C^R_H \Gamma_{co,H}\, \langle |S_{HH}|^2 \rangle}{P_V C^T_V W^2_V (G^A_V)^2 LNA_V\, C^R_V \Gamma_{co,V}\, \langle |S_{VV}|^2 \rangle} \quad (1)$$

$$LDR^m_h = \frac{W_V G^A_V LNA_V\, C^R_V \Gamma_{x,V} G^R_x\, \langle |S_{VH}|^2 \rangle}{W_H G^A_H LNA_H\, C^R_H \Gamma_{co,H} G^R_{co}\, \langle |S_{HH}|^2 \rangle} \quad (2)$$

where Z^m_{dr} and LDR^m_h are measured differential reflectivity and linear depolarization ratio, respectively, and where $\Gamma_{co,V}, \Gamma_{co,H}, \Gamma_{x,V}$ represent the insertion losses associated with various paths through the IF switch. For example, $\Gamma_{co,V}$ represents the path from the V IF-switch input through the switch to the copolar receiver. Note that $\langle |S_{HH}|^2 \rangle / \langle |S_{VV}|^2 \rangle = Z_{dr}$ and $\langle |S_{VH}|^2 \rangle / \langle |S_{HH}|^2 \rangle = LDR_h$ are the intrinsic values we wish to isolate with $\langle * \rangle$ denoting time average. The ratio of the crosspolar powers becomes,

$$\frac{R_{xv}}{R_{xh}} = \frac{P_V C^T_V LNA_H\, C^R_H \Gamma_{x,H}\, \langle |S_{HV}|^2 \rangle}{P_H C^T_H LNA_V\, C^R_V \Gamma_{x,V}\, \langle |S_{VH}|^2 \rangle} \quad (3)$$

where R_{xv} and R_{xh} represent the broadcast V receive H and broadcast H receive V crosspolar powers, respectively. By reciprocity $\langle |S_{HV}|^2 \rangle = \langle |S_{VH}|^2 \rangle$ and these terms cancel. This ratio should be unity so that the remaining terms represent the radar components that cause any deviation of the ratio from unity. There are four sun calibration measurements,

$$H_{co,s} = G^A_H W_H LNA_H\, C^R_H \Gamma_{co,H} G^R_{co} \quad (4)$$

$$V_{co,s} = G^A_V W_V LNA_V\, C^R_V \Gamma_{co,V} G^R_{co} \quad (5)$$

$$H_{x,s} = G^A_H W_H LNA_H\, C^R_H \Gamma_{x,H} G^R_x \quad (6)$$

$$V_{x,s} = G^A_V W_V LNA_V\, C^R_V \Gamma_{x,V} G^R_x \quad (7)$$

where the subscript "co,s" and "x,s" represent the H and V sun powers received in the copolar and crosspolar power receivers, respectively. In order to calibrate Z^m_{dr} (and LDR^m_h), the three following solar ratios are needed:

$$\mathcal{S}_1 = V_{co,s}/H_{co,s} = \frac{G^A_V W_V LNA_V\, C^R_V \Gamma_{co,V}}{G^A_H W_H LNA_H\, C^R_H \Gamma_{co,H}} \quad (8)$$

$$\mathcal{S}_2 = V_{x,s}/H_{x,s} = \frac{G^A_V W_V LNA_V\, C^R_V \Gamma_{x,V}}{G^A_H W_H LNA_H\, C^R_H \Gamma_{x,H}} \quad (9)$$

$$\mathcal{S}_3 = V_{x,s}/H_{co,s} = \frac{G^A_V W_V LNA_V\, C^R_V \Gamma_{x,V} G^R_x}{G^A_H W_H LNA_H\, C^R_H \Gamma_{co,H} G^R_{co}} \quad (10)$$

Then for the FHV (fast alternating H and V transmission) S-Pol configuration, Z^m_{dr} and LDR^m_h can be calibrated using,

$$LDR_h = LDR^m_h \frac{1}{\mathcal{S}_3} \quad (11)$$

$$Z_{dr} = Z^m_{dr}\, \mathcal{S}_1\, \mathcal{S}_2\, \frac{R_{xv}}{R_{xh}} \quad (12)$$

Thus the Z_{dr} bias is defined as

$$Z^{bias}_{dr} = \mathcal{S}_1 \mathcal{S}_2\, \frac{R_{xv}}{R_{xh}} \quad (13)$$

The $\mathcal{S}_1\mathcal{S}_2$ ratio is

$$\mathcal{S}_1\mathcal{S}_2 = \frac{(G^A_V W_V LNA_V\, C^R_V)^2 \Gamma_{co,V} \Gamma_{x,V}}{(G^A_H W_H LNA_H\, C^R_H)^2 \Gamma_{co,H} \Gamma_{x,H}} \quad (14)$$

The test pulses injected at the test plane yield the following power ratios,

$$\mathcal{T}_1 = V_{co}/H_{co} = \frac{LNA_V\, C^R_V \Gamma_{co,V}}{LNA_H\, C^R_H \Gamma_{co,H}} \quad (15)$$

$$\mathcal{T}_2 = V_x/H_x = \frac{LNA_V\, C^R_V \Gamma_{x,V}}{LNA_H\, C^R_H \Gamma_{x,H}} \quad (16)$$

$$\mathcal{T}_3 = V_x/H_{co} = \frac{LNA_V\, C^R_V \Gamma_{x,V} G^R_x}{LNA_H\, C^R_H \Gamma_{co,H} G^R_{co}} \quad (17)$$

These test pulse ratios can be used with the above solar ratios for consistency and to analyze Z_{dr} variability caused by associated RF/IF components. For example, $\mathcal{S}_1$ can be compared to $\mathcal{T}_1$. If the experimental measurement of these two ratios vary differently versus time then the source of variability can be assigned to non common components, namely the ratio, $G^A_V W_V / G^A_H W_H$ or the test pulse generator itself.

3. Data Analysis

Solar scan data were gathered on December 24, 26, 2014 and January 9, 10, 11,12, 15, and Feb.

22, 25, 26, 27, 2015. There are 328 analyzed solar scans. The transmitter was on during the solar scans so that both a ratio of crosspolar powers as well as the solar radiation powers could be estimated. The solar powers were estimated from gates beyond 100 km range. The crosspolar power ratio was estimated from gates close to the radar where side lobes yielded significant ground clutter power. The temperate at S-Pol was estimated from MADIS weather stations located relatively close to S-Pol. While this temperature will be somewhat different than the actual environment temperature at S-Pol, it is close and does track the trends of temperature. Shown in Fig. 3 is the Z_{dr} bias as a function of temperature at S-Pol. Clearly there is a trend in the data with the Z_{dr} bias varying 0.4 dB over the temperature range of -20°C to 20°C. This is approximately 0.01 dB /(deg. C).

It is of interest to identify the hardware components of S-Pol that cause this variation. The two components of the Z_{dr} bias estimate are 1) the solar ratio $\mathcal{S}_1\mathcal{S}_2$ and the crosspolar power ratio R_{xh}/R_{xv}. Shown in Figs. 4 and 5 are scatter plots of these two ratios again versus temperature. The scatter plot of $\mathcal{S}_1\mathcal{S}_2$ is very similar to Fig. 3 and shows about 0.4 dB variation versus temperature. The scatter plot of the crosspolar power (XP) ratio does not show a similar trend versus temperature. The XP ratio varies only about 0.05 dB. From these plots, we conclude that most of the variance in the Z_{dr} bias as a function of outside temperature likely comes from the antenna and accompanying waveguide down to the S-Pol transmitter container rather than the receive electronics. The transmitter and receiver electronics are located in the transmitter container with a temperature controlled environment.

3.1. *Variation Analysis*

Here we compare various solar, test pulse and crosspolar power ratios in order to identify the radar components that are most likely to be causing the Z_{dr} calibration variance over time.

Figure 6 shows V_{co}/V_x and H_{co}/H_x power ratios for both solar and test pulse data from 4 days. From Fig. 2 the powers are,

$$V_{co}/V_x = \frac{\Gamma_{co,V} G^R_{co}}{\Gamma_{x,V} G^R_x} \quad (18)$$

$$H_{co}/H_x = \frac{\Gamma_{co,H} G^R_{co}}{\Gamma_{x,H} G^R_x} \quad (19)$$

These equations are valid for either the solar or test pulse powers. Thus these ratios are only a function of the receive path from the IF switch through the receivers. The V_{co}/V_x for both the test pulse and solar scans should be identical but there is a small difference of about 0.01 dB on average. On Jan. 9 and 15, V_{co}/V_x and H_{co}/H_x were flat during the measurement period while there is a slight increase in these ratios for Feb. 6 and 20 of about 0.005 dB. The conclusion is that solar power ratio tracks the test pulse power ratio and there is negligible change in the mean values versus time due to the corresponding hardware components (i.e., the IF switch and the RVP8 receiver). The top two plots of Fig. 6 also show curves H_{co}/H_x which are offset from V_{co}/V_x by about a tenth of a dB. This tenth of a dB is caused by the V_x signal and the $\Gamma_{x,V}$ IF switch path.

We next compare the measurement of the transmit power to the crosspolar power ratio. The transmit V/H power ratio measured at the test plane is

$$P_{tx} = \frac{P_{tx,v}}{P_{tx,h}} = \frac{P_V C^T_V}{P_H C^T_H} \quad (20)$$

and this ratio is contained in the crosspolar power ratio of Eq.(3). Thus variations in the P_{tx} should also be seen in R_{xv}/R_{xh}. Figure 7 shows P_{tx} and R_{xv}/R_{xh} for four days as labeled and the two curves correlate (i.e., similar trends versus time) quite well except for the 9 January data. However for this day, the right and left vertical scales are just 0.02 dB and 0.015 dB in extent, respectively. The time duration is over 5 hours. Thus, it is apparent that for these four days the variability of the transmit powers is the dominate factor in the variability of the crosspolar power ratio (especially 6 Feb and 15 Jan.) and the RF components are the transmit power divider (fast mechanical switch) and the circulators on transmit. Figure 8 shows R_{xv}/R_{xh} and the difference (in dB) $R_{xv}/R_{xh} - P_{tx}$. Using Eqs.(3) and (20), this difference is (in dB),

$$\frac{R_{xv}}{R_{xh}} - P_{tx} = \frac{LNA_H\, C^R_H \Gamma_{x,H}}{LNA_V\, C^R_V \Gamma_{x,V}}. \quad (21)$$

From above, since the paths through the IF switch contribute very little to Z_{dr} variance, we conclude that the variance in this difference curve is attributable to the LNAs and circulators on receive. This difference is only 0.02 dB to .03 dB over each day. It is likely that the circulators would behave similarly on receive as they do on transmit. If this is true then the increasing trend in the crosspolar power ratio for 6 February and for 15 January is due to the transmit power divider circuit. This increase is about 0.05 dB for both days.

3.2. *A Comparison of Vertical Pointing and Crosspolar Z_{dr} Calibrations*

Calibrating Z_{dr} is especially challenging since there is no calibration standard by which to judge the estimated Z_{dr} calibration figure. It is popularly assumed that vertical pointing data in rain yields the correct Z_{dr} calibration. Previous S-Pol measurements have shown that the Z_{dr} calibration number from the VP and CP technique agreed well (Hubbert and Dixon 2012). Here we present three more comparisons between VP and CP. Figure 9 show a Z_{dr} histogram from VP measurements (top panel) and a solar power antenna pattern from which the CP Z_{dr} calibration is calculated both gathered in close time proximity on 22 February 2015. Several more solars scans and VP scans were also made during this time. Additionally, on February 25 and 26, 2015, VP data were gathered in close time proximity to solar scans. The average results are

- From 22 Feb. Z_{dr_cor} = -0.046 dB and the VP Z_{dr} mean = 0.046 dB
- From 25 Feb. Z_{dr_cor} = 0.1 dB and the VP Z_{dr} mean = 0 dB
- From 26 Feb. Z_{dr_cor} = 0.075 dB and the VP Z_{dr} mean = 0.02 dB

where Z_{dr_cor} is the CP Z_{dr} correction factor for the CP technique. By definition is should be the negative of the Z_{dr} calibration number from the VP technique. Thus, the CP and VP Z_{dr} calibration numbers agree for the 22 February case while they disagree by about a tenth of a dB for the 25 and 26 February cases.

4. Discussion

From the above analysis it is apparent that for the data cases presented here, it is the differential path from the antenna down to the test plane that is responsible for the largest variation in the Z_{dr} calibration number when the antenna is exposed to large temperature changes. This variation in Z_{dr} was well correlated to the environmental temperature at the S-Pol site, increasing 0.01 dB/(deg. C). The Z_{dr} variance due to the differential path from the test plane through the RVP8 receiver is remarkably constant in comparison. This runs contrary to the widely held belief that it is only the active portion of the receiver chain that needs to be monitored for Z_{dr} calibration updates. S-Pol data presented here shows the non-active portion of the receiver path (i.e., antenna and waveguide down to the test plane) causes large variations in Z_{dr} calibration as a function of the outside temperature.

A possible explanation for this can be gleaned from Z_{dr} solar patterns gathered at several receive frequencies. Figures 10 to 14 show the Z_{dr} antenna patterns for frequencies 2790, 2795, 2800, 2805 and 2809 MHz. The two white circles mark the 1° and 2° solid angles. As can be seen the Z_{dr} patterns change significantly as a function of frequency and thus the Z_{dr} calibration number (in part the integration over the Z_{dr} pattern) changes also.

Figure 15 shows the S_1S_2 calibration number as a function of solars scans from 20 February 2015 with the solid angle integration over the S_1S_2 pattern as a parameter. Shown are integrations for solid angles: A) 1°, B) 1.25°, C) 1.5°, D) 1.75°, E) 2.0°. As can be seen the curve a 1° integration shows a small deviation from the rest of the curves. For solid angles greater than or equal to 1.25°, there is little variation among them. This consistency among the S_1S_2 integrations as a function of index shows that the integrations of solid angles $\geq 1.25^\circ$ converge and the integration over 1.25° is sufficient to capture the variability of the Z_{dr} antenna pattern.

Since the Z_{dr} calibration number is highly correlated to environmental temperature, it is possible that thermal expansion of the antenna parabolic reflector causes the variance of the Z_{dr} calibration number. To make a first order estimate of the amount of antenna dish movement required for a significant change in Z_{dr} calibration number, we first consider the phase difference incident at the focal point of the antenna for a 1 MHz change in receive frequency. It has been observed that the S_1S_2 antenna pattern can indeed change significantly for a 1 MHz change in receive frequency. Using 2800 and 2801 MHz, this gives 35.5727 and 35.560 wavelengths from the feed horn to the dish apex for a difference of 0.0127 wavelengths. This translates to a phase difference of 4.57° and a wavelength difference of 1.37mm. We assume that this is the source of the variation in the S_1S_2 antenna patterns and thus now ask whether or not the thermal expansion of the dish is sufficient to make such a change in dimension. A typical thermal expansion coefficient for aluminum alloy is 23.6 μcm/cm/(deg. C). The S-Pol support struts are about 16 feet long so that for a change of 10°C, this translates to an expansion of 1.15 mm, which is of the same order of magnitude as 1.37 mm. While this is not proof that the thermal expansion of the S-Pol antenna is the cause of the Z_{dr} calibration variance as a function of temperature, it does show that it is physically possible.

As a final note, in 2009 NCAR made photogram-

metric measurements of the S-Pol antenna, struts and feed horn in order to determine the shape of the parabolic reflector and the RMS error of the reflector. These measurements showed that the feed horn drooped 0.9 mm when comparing vertical pointing position (90°) to a horizontal position (0°). Additionally, the focal length changed by 1.4 mm. These changes in dimension are small but could cause a significant difference in the Z_{dr} antenna pattern (as shown above) and thus cause the Z_{dr} calibration number to be different by a tenth of a dB or more for the vertical and horizontal antenna positions. This then has a significant implication for Z_{dr} calibration: the CP technique is preferable to the VP technique because it can be executed while the antenna is in a more horizontal position where it will be for most precipitation measurements.

5. Conclusions

The data presented here indicates that the Z_{dr} bias of S-Pol is correlated to the outside temperature at S-Pol. Analysis of the solar power ratios, copolar power ratios and test pulse data shows that this variation is due to the receive path from the antenna down into the test plane in the transmitter trailer. This variation in the the Z_{dr} calibration number is about 0.01° dB/C. Thus for every 10°C change in temperature, the Z_{dr} calibration could change by about 0.1 dB. In contrast, the active portion of the receive path, i.e., from the circulators to the RVP8 receiver, showed very little variance over the days examined here. The second most significant source of variation in the Z_{dr} calibration number was the transmit power division network. These results have implications for NEXRAD Z_{dr} calibration as well as for other weather radars.

Acknowledgment This research was supported in part by the ROC (Radar Operations Center) of Norman OK. The National Center for Atmospheric Research is sponsored by the National Science Foundation. Any opinions, findings and conclusions or recommendations expressed in this publication are those of the authors and do not necessarily reflect the views of the National Science Foundation.

References

Hubbert, J., V. Bringi, and D. Brunkow, 2003: Studies of the polarimetric covariance matrix: Part I: Calibration methodology. *J. Atmos. Oceanic Technol.*, **20**, 696–706.

Hubbert, J. C. and M. Dixon: 2012, z_{dr} calibration for radars that transmit simultaneous horizontal and vertical polarizations. *Proceedings 28th Conference on Interactive Information Processing Systems, IIPS*, Amer. Meteor. Soc., New Orleans, LA.

Saxon, D.S., 1955: Tensor scattering matrix for the electromagnetic field. *Phys. Rev.*, **100**, 1771–1775.

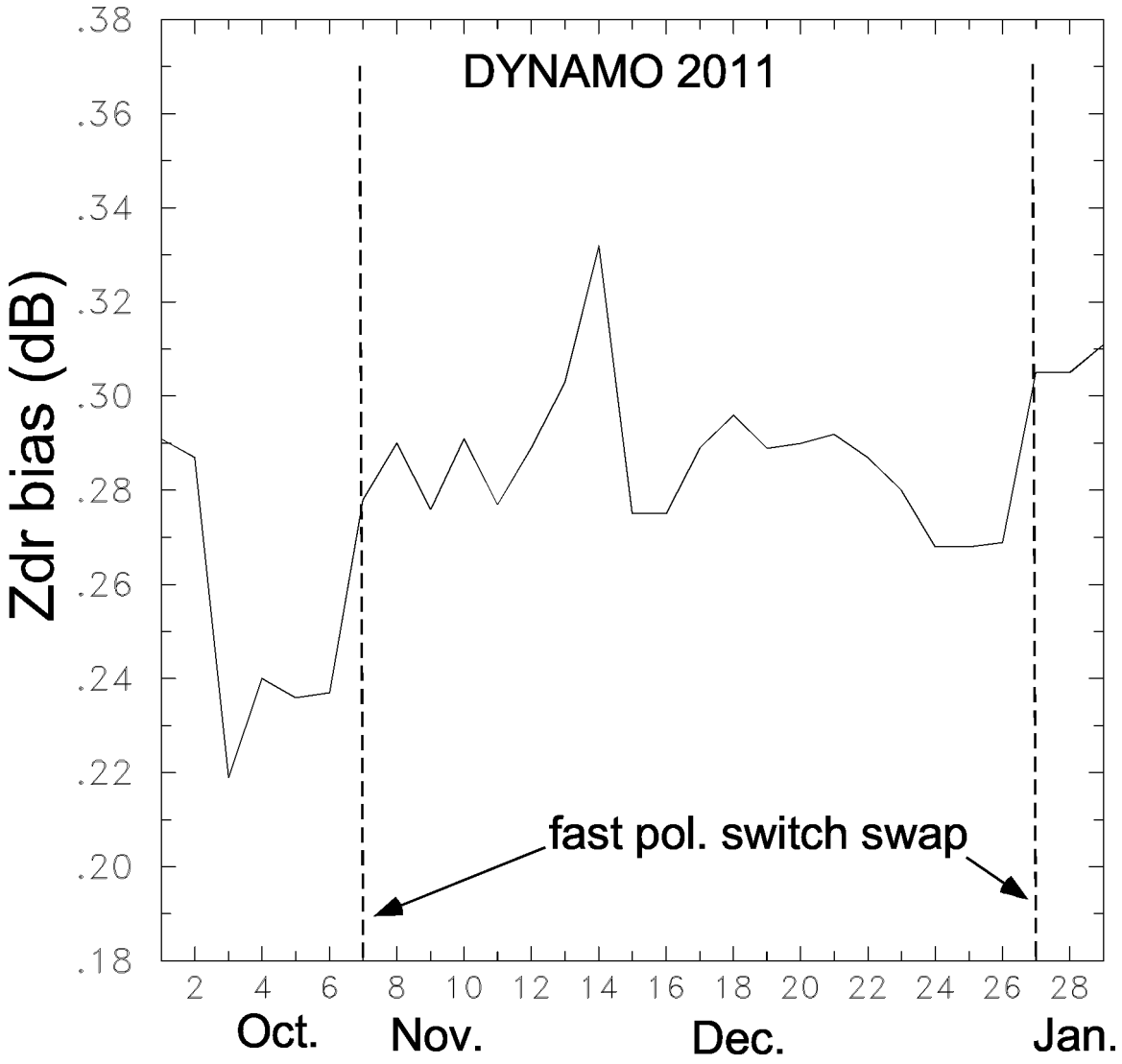

Figure 1: *S-Pol Z_{dr} calbrations estimated from vertical pointing data in rain during the experiment DYNAMO in the Maldives, 2011 to 2012. The temperature at S-Pol during these measurements was about 25°C $\pm 2°$. The dashed vertical lines indicate times when the fast polarization switched was replaced.*

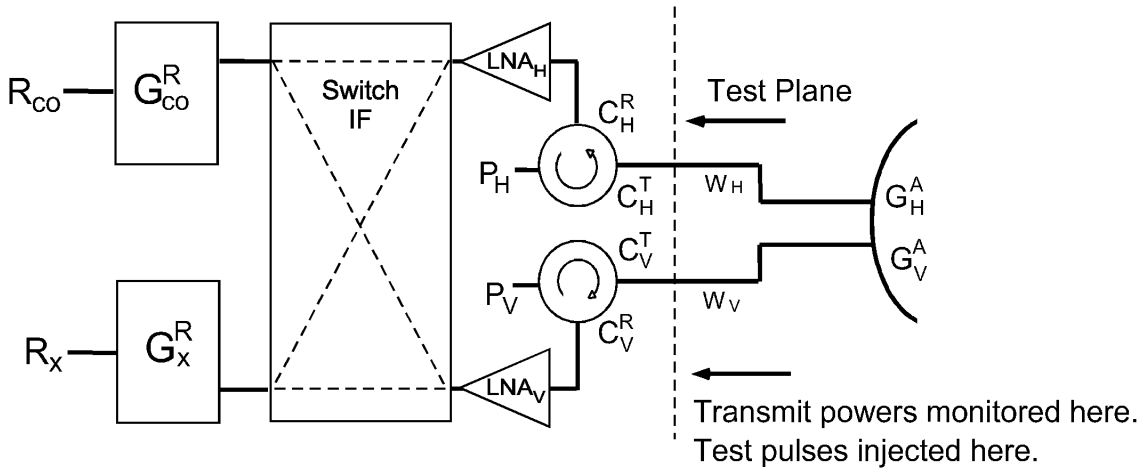

Figure 2: *Block diagram of part of the S-Pol radar receiver section. H and V signals can be directed to either the co- or cross-receiver. The mechanical switch is not shown.*

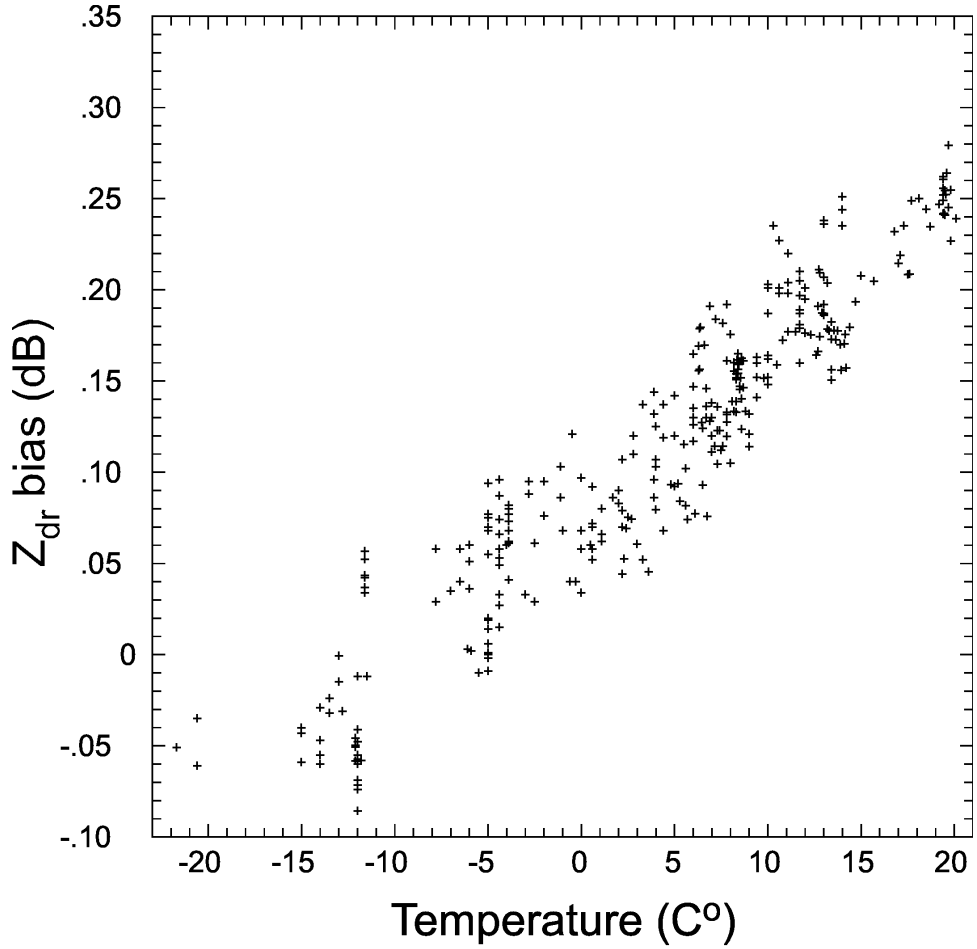

Figure 3: *Scatter plot of Z_{dr} bias calculated from 328 solar scans gathered by S-Pol as a function of the outside temperature at S-Pol.*

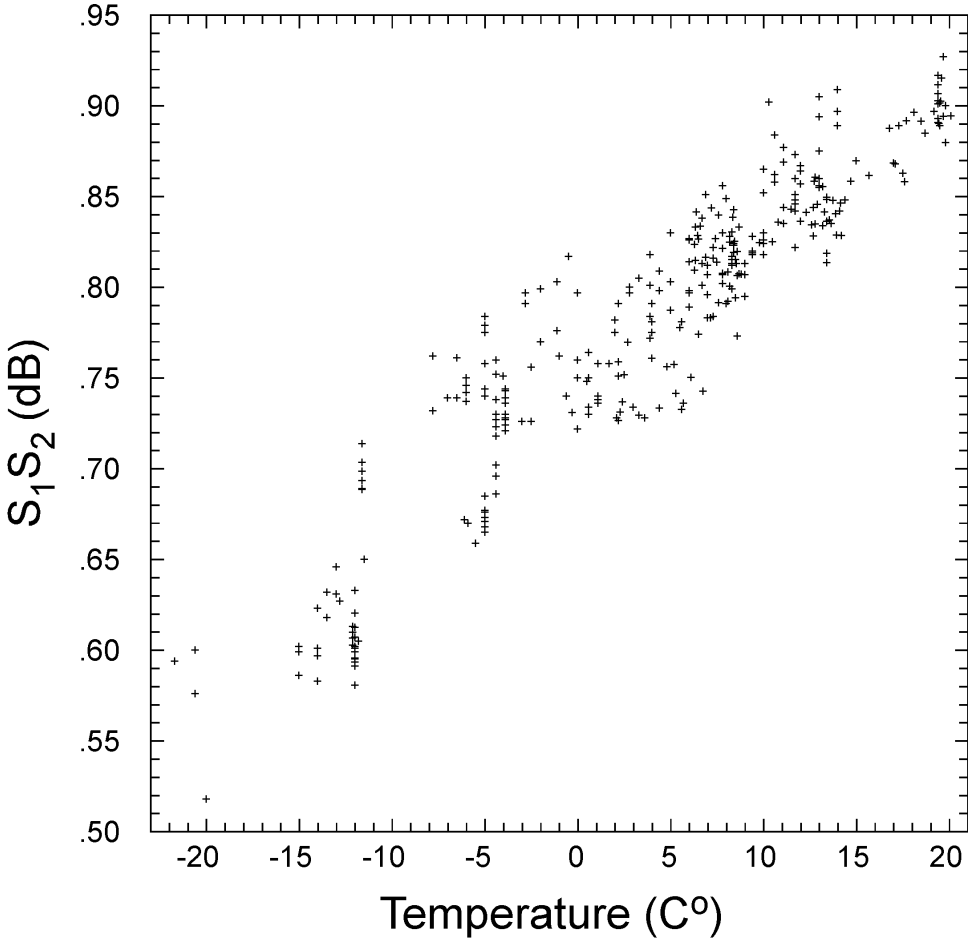

Figure 4: *Scatter plot $\mathcal{S}_1\mathcal{S}_2$ corresponding to Fig. 3.*

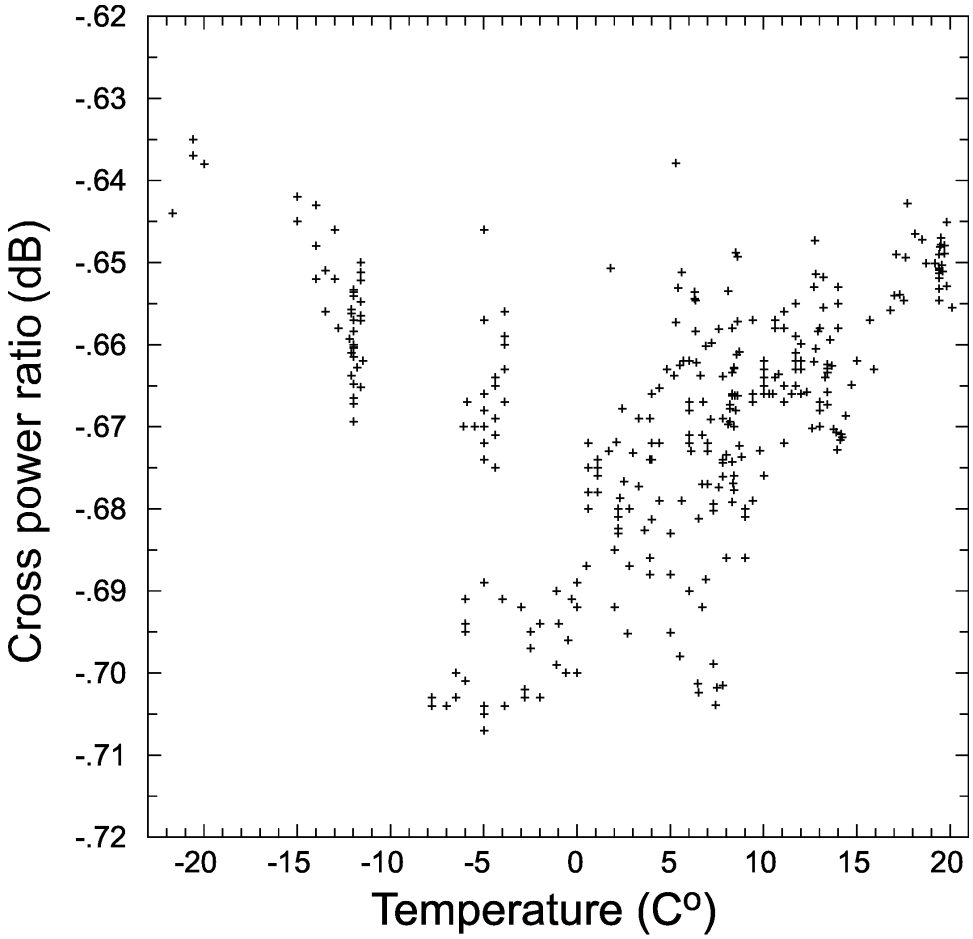

Figure 5: *Scatter plot of the crosspolar power ratio calculated from 328 solar scans gathered by S-Pol as a function of the outside temperature at S-Pol.*

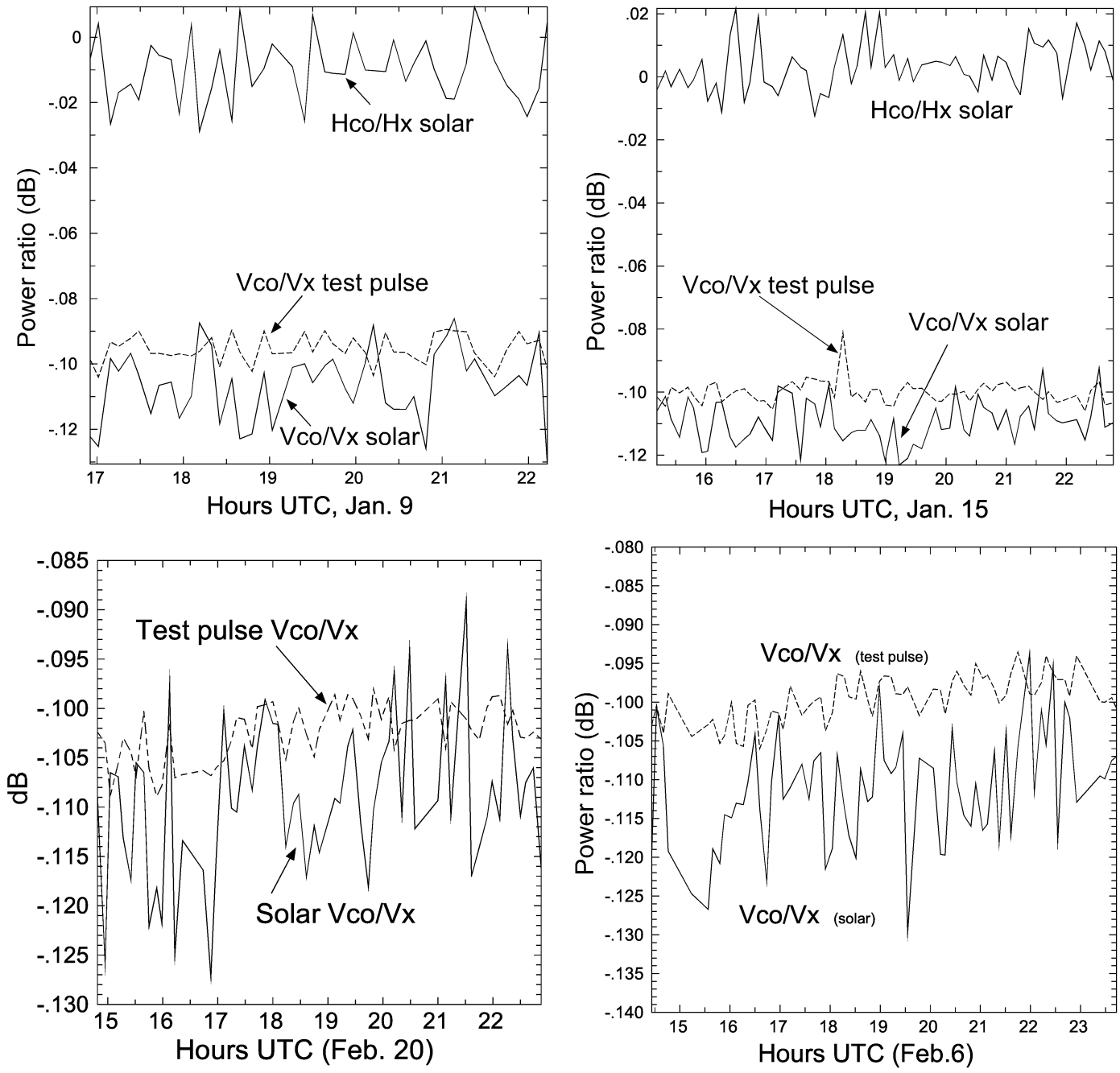

Figure 6: *Vco/Vx and Hco/Hx for both solars and test pulse data for 4 days.*

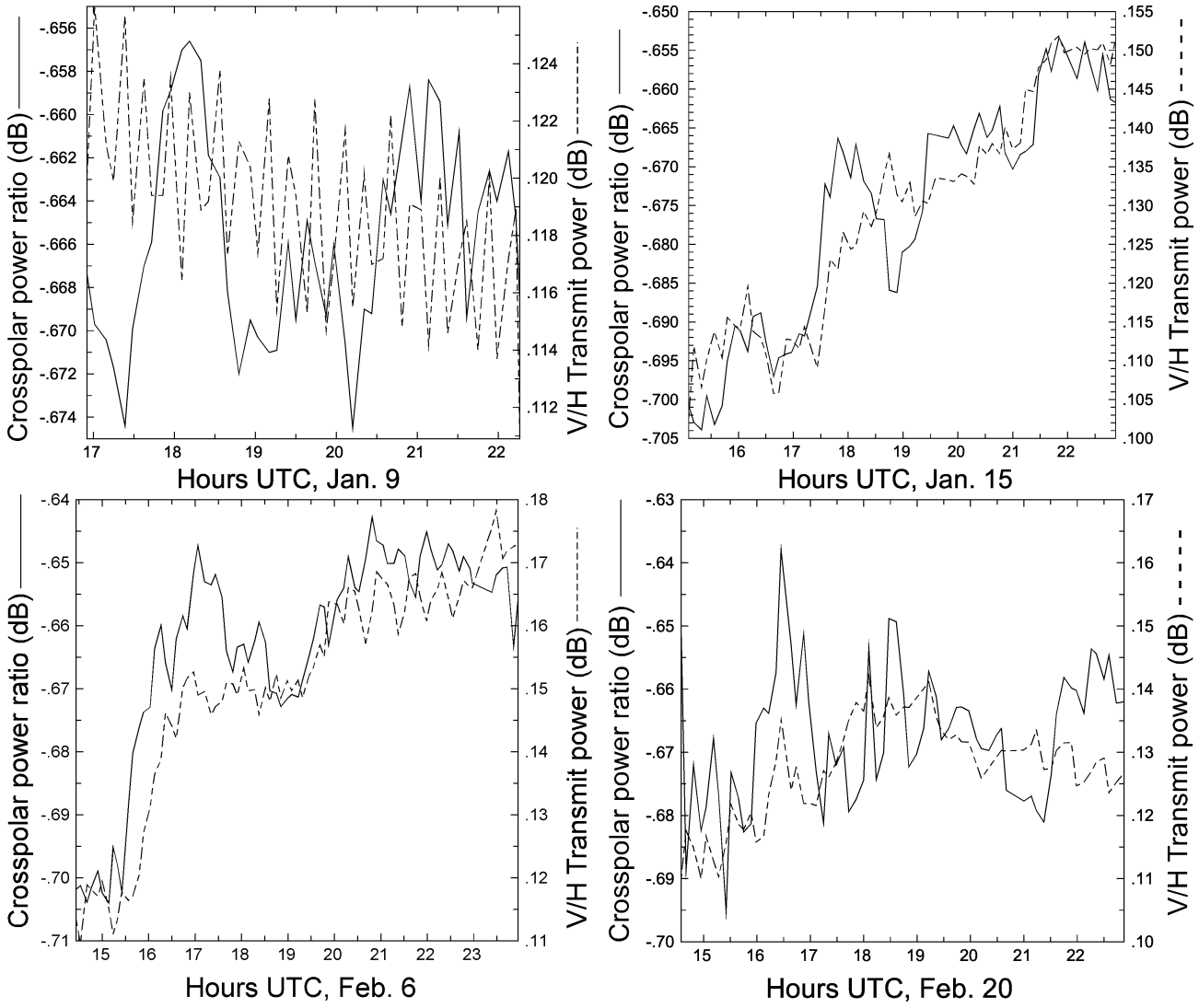

Figure 7: *Crosspolar power ratio (solid line) and the V/H transmit power ratio for 4 days.*

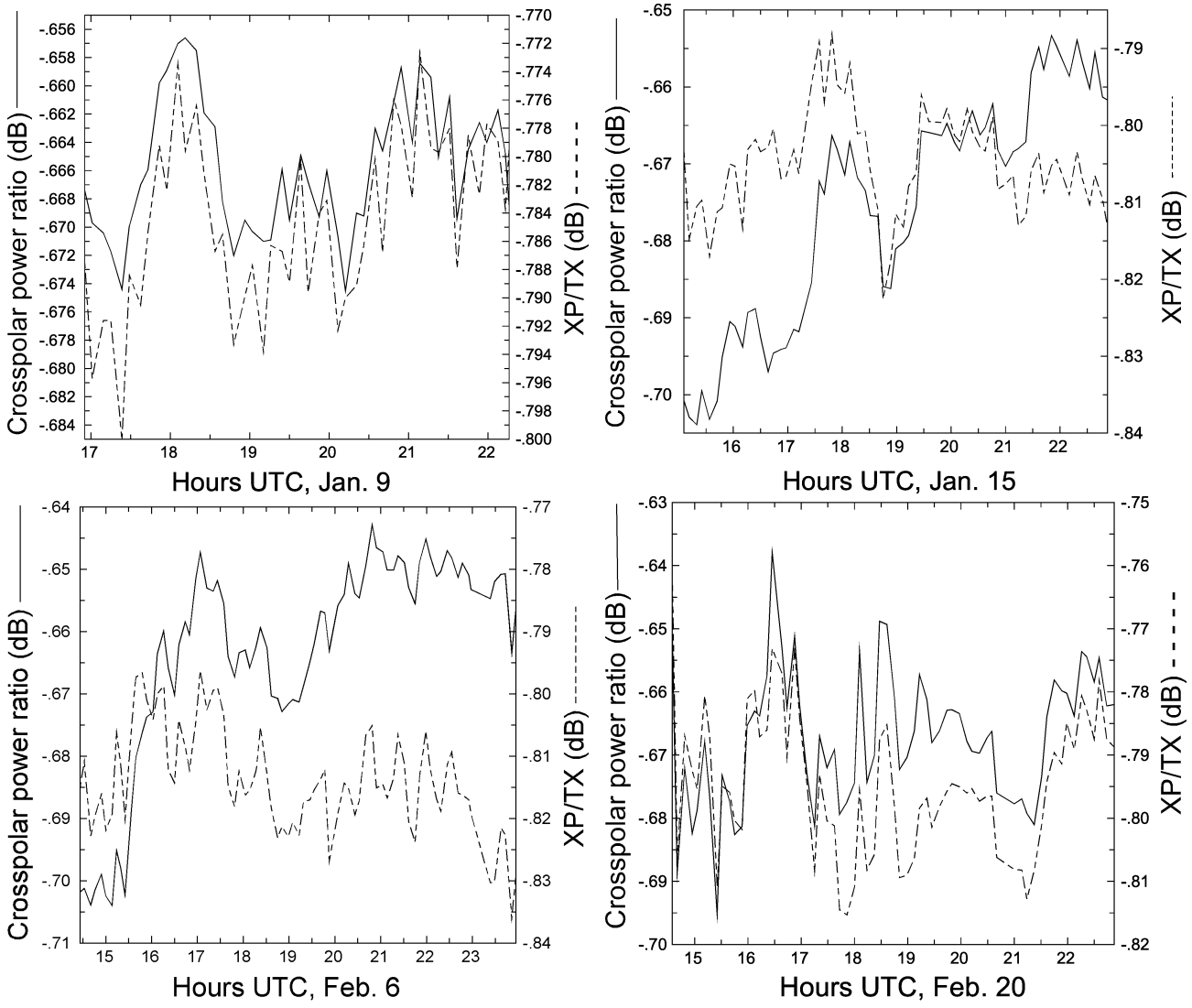

Figure 8: *Crosspolar power ratio (solid line) and the difference of the crosspolar power ratio and V/H transmit power ratio (in dB) for 4 days.*

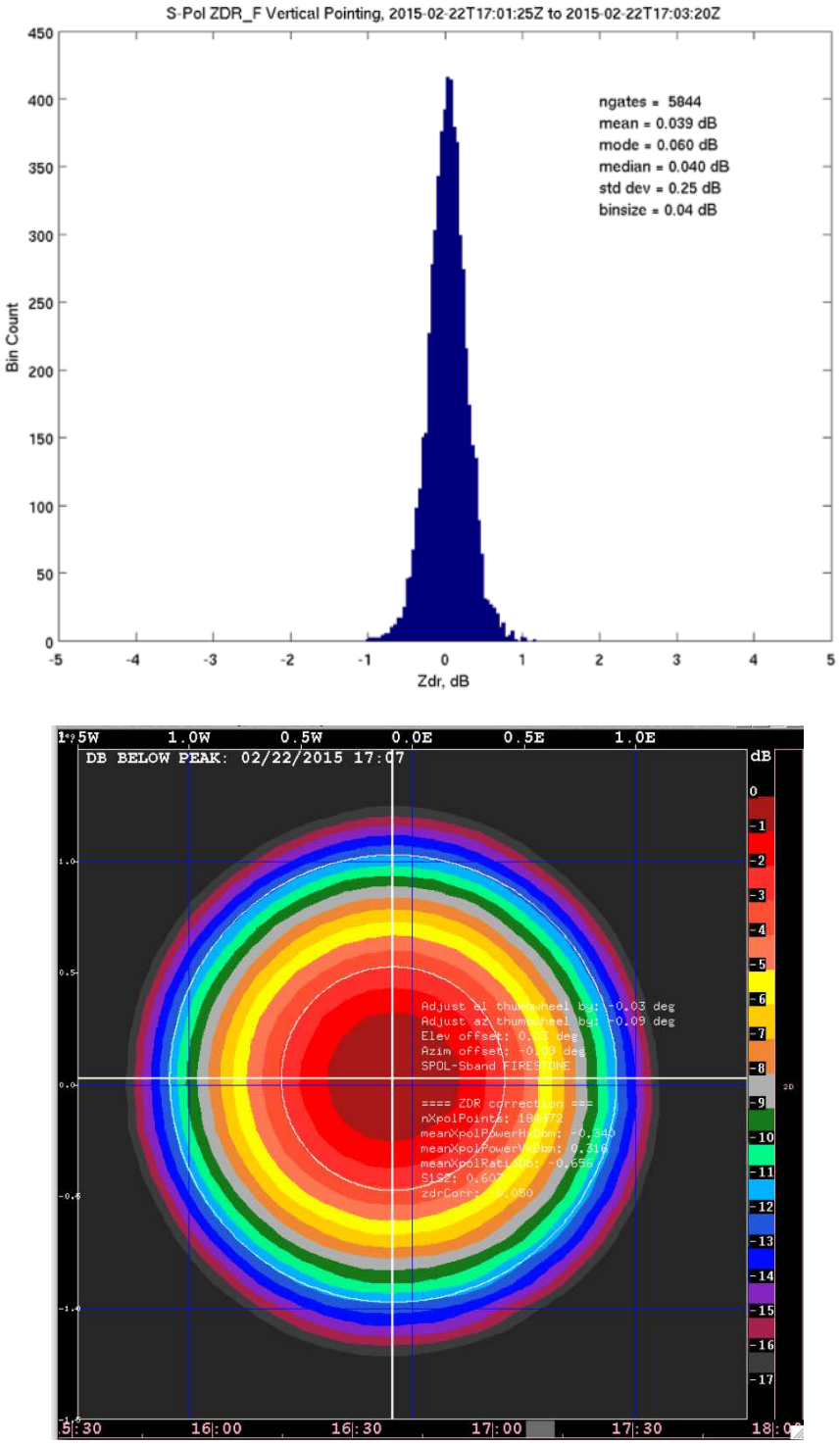

Figure 9: *A comparison of vertical point (VP) and crosspolar power (CP) Z_{dr} calibration. Top: VP Z_{dr} histogram. Bottom: H-power solar antenna pattern.*

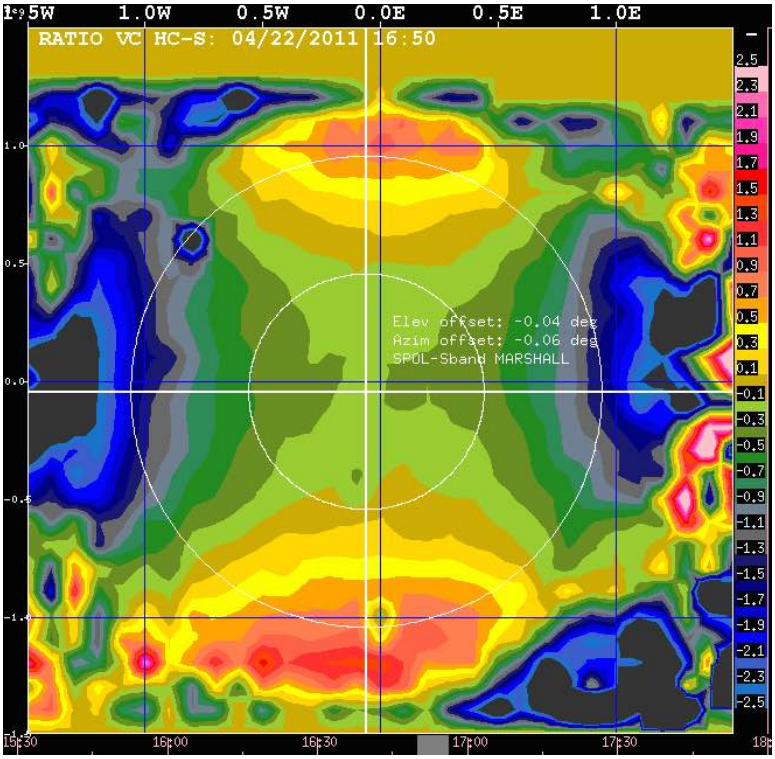

Figure 10: *A Zdr solar antenna pattern measured at 2790 MHz.*

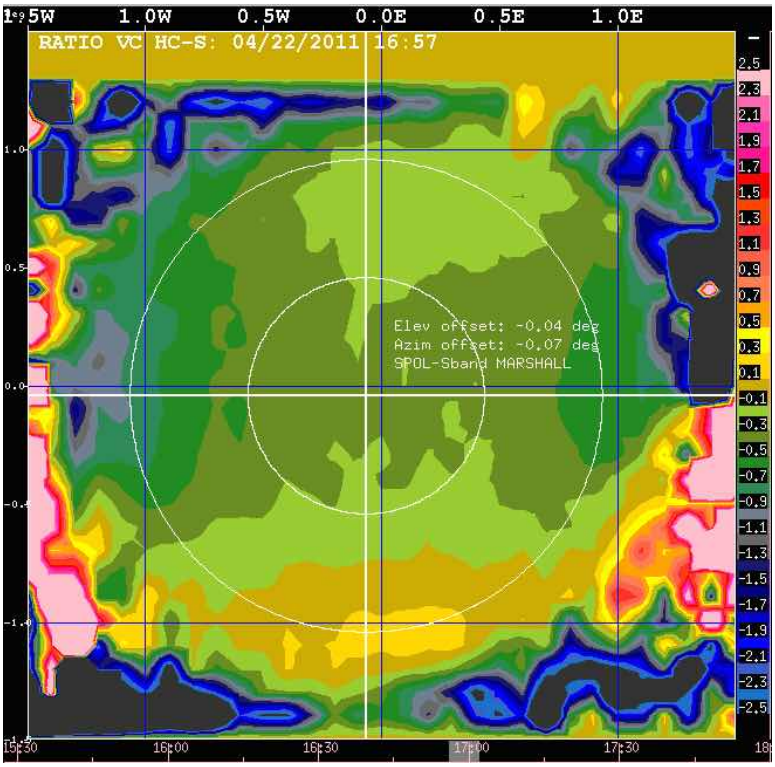

Figure 11: *A Zdr solar antenna pattern measured at 2795 MHz.*

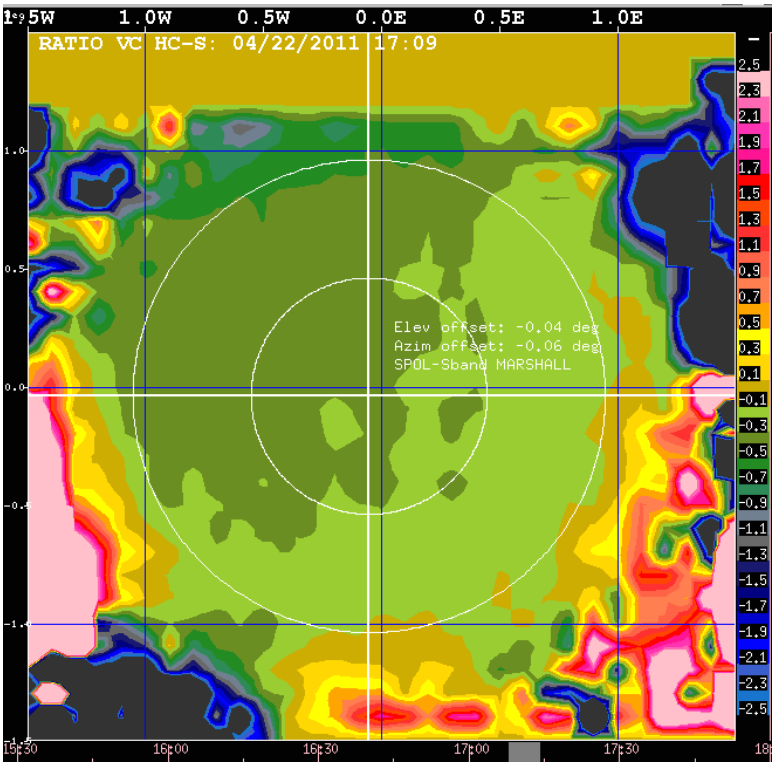

Figure 12: *A Zdr solar antenna pattern measured at 2800 MHz.*

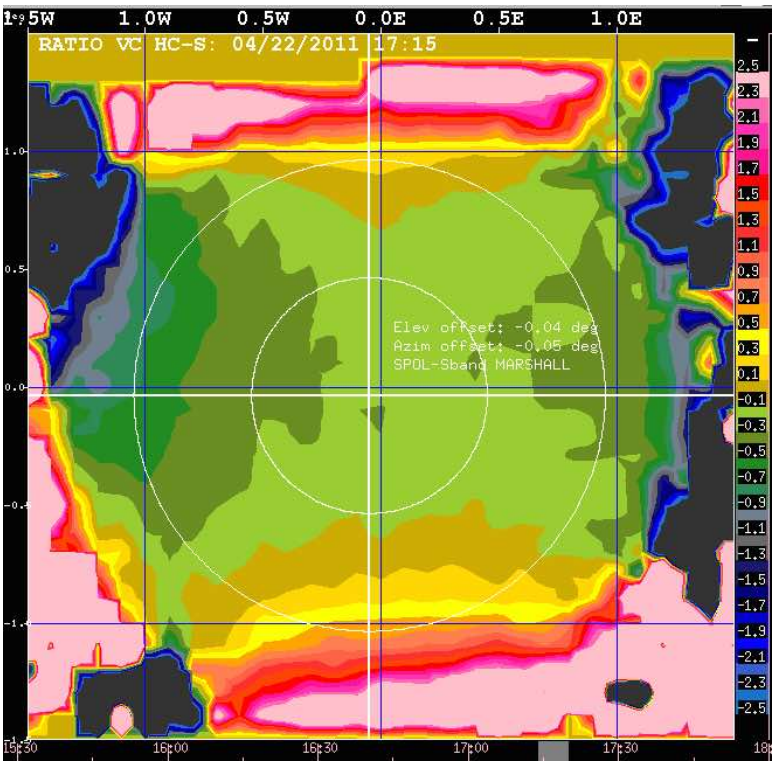

Figure 13: *A Zdr solar antenna pattern measured at 2805 MHz.*

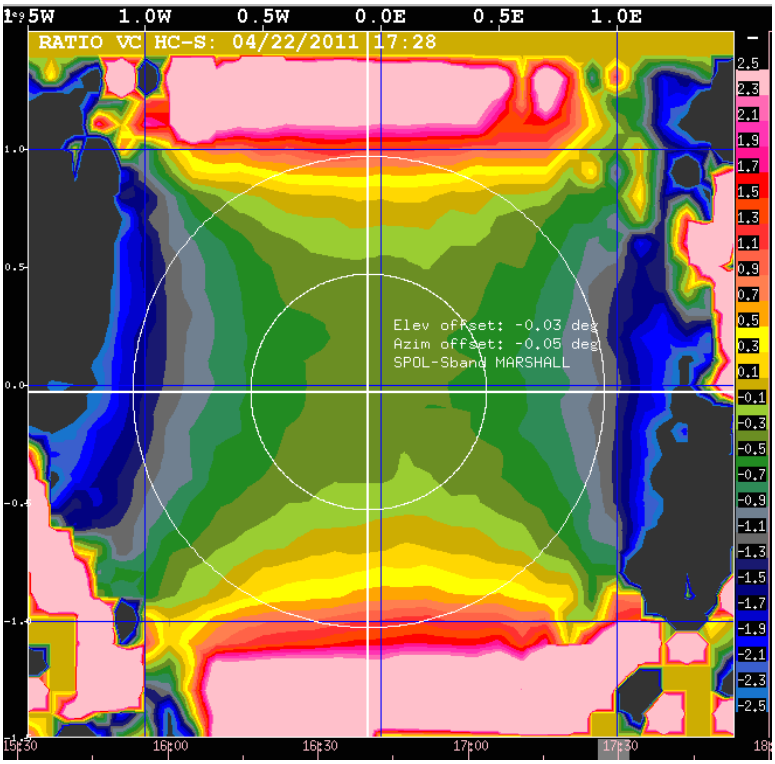

Figure 14: *A Zdr solar antenna pattern measured at 2809 MHz.*

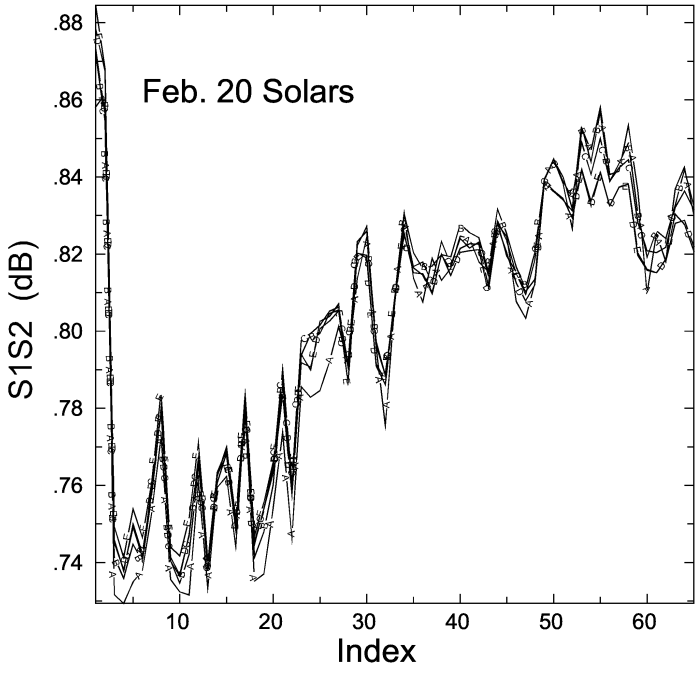

Figure 15: *Vco/Hco solars for various annuli of integration: (A)* 1°*, (B)* 1.25°*, (C)* 1.5°*, (D)* 1.75°*, (E)* 2°*.*